Chain-oxygen ordering in twin-free $YBa_2Cu_3O_{7-\delta}$ single crystals driven by 20-keV electron irradiation

H. W. Seo,[1,*] Q. Y. Chen,[1,†] M. N. Iliev,[1] Tom H. Johansen,[1,3] N. Kolev,[1,‡] U. Welp,[2] C. Wang,[1] and Wei-Kan Chu[1]
[1]*Department of Physics and Texas Center for Superconductivity, University of Houston, Houston, Texas, USA*
[2]*Argonne National Laboratory, Argonne, Illinois, USA*
[3]*Department of Physics, University of Oslo, P. O. Box 1048, Blindern, 0316 Oslo, Norway*
(Received 4 March 2005; published 4 August 2005)

We have examined the effects of 20-keV electron irradiation on the $[\text{-Cu(1)-O(1)-}]_n$ chain-oxygen arrangements in oxygen-deficient but otherwise twin-free $YBa_2Cu_3O_{7-\delta}$ single crystals. Comparison of polarized Raman spectra of nonirradiated and irradiated areas provides evidence that electron bombardments instigate the collective hopping of oxygen atoms either from an interstitial at O(5) site to a vacant O(1) chain site or by reshuffling the chain segments to extend the average length of chains without changing the overall oxygen content. This oxygen ordering effect, while counterintuitive, is analogous to that found in photoexcitation-induced ordering in which temporal charge imbalance from electron-hole pair creation by inelastic scattering of incident electrons causes a local lattice distortion which brings on the atomic rearrangements.

DOI: 10.1103/PhysRevB.72.052501 PACS number(s): 74.72.−h, 74.40.+k, 64.60.Cn, 81.30.Hd

Recent observations of photoexcitation-induced superconductivity and persistent normal-state photoconductivity in $YBa_2Cu_3O_{7-\delta}$ (YBCO) have revealed an intriguing phenomenon involving the ordering of $[\text{-Cu(1)-O(1)-}]_n$ chain-oxygen atoms.[1–3] Such ordering yields longer chains with larger n and higher carrier concentration on the $Cu(2)O(3)_2$ planes because longer chain fragments are more effective in hole doping. Therefore, it also results in a higher superconducting transition temperature T_c for the same overall oxygen stoichiometry.[1–4] While the detailed ordering mechanism is still under debate, it is believed[1] that local photoexcitation of electronic states in atoms leads to a fluctuation of thermodynamic potential in the nearby regions, thus providing a reduced activation energy barrier for atomic migration. Theoretical investigations made on the thermodynamics of oxygen ordering in YBCO based on a two-dimensional Ising model and its variants[3,5] have shown that, indeed, ordered superpatterns of nonsegmented CuO chains on the CuO-chain planes are energetically favorable. This was corroborated by the observation of cell-doubled (O-II or Ortho-II) or cell-tripled (O-III or Ortho-III) phases in both oxygen-deficient YBCO bulk crystals and thin films using neutron scattering, x-ray and electron diffraction, and electrical transport measurement.[6–8]

The incident photon energy and energy transfer involved in the above-mentioned photoexcitation was in the range of 2–3 eV.[1–4,9] This compelled us to ask whether an electron beam that imparts the same energy to an oxygen atom would bring about a similar ordering effect. Assuming the energy transfer comes directly from knock-on impacts, the required incident electron energy would then be 10–30 keV, which is readily available on commercial scanning electron microscopes. Electron irradiation, however, has been widely known to create crystal defects, e.g., by 100 keV–1 MeV electron bombardments on YBCO superconductors.[10,11] At such higher energies, however, CuO_2-plane oxygen defects may be generated and their effects could also offset contributions from the CuO-chain defects. Therefore, there is a need to verify the effects for irradiation energies which are so low that only the kinetics of the chain oxygen is relevant. For this reason, we designed a comparative study via micro-Raman spectroscopy on a twin-free oxygen-deficient YBCO single crystal subjected to a 20-keV electron bombardment. By comparing the spectra from irradiated and nonirradiated areas, we find that this irradiation causes a healing of existing point defects on the CuO chains and enhances the oxygen ordering.

Single crystals of YBCO were prepared by a flux-growth technique, followed by slow cooling to room temperature to minimize residual strain. The crystal selected for detailed measurements was 0.05 mm thick with lateral dimensions of 1×0.7 mm^2. A micrograph of the crystal taken under a polarized light microscope is shown in Fig. 1(a), where it is evident that the sample has several large twin-free domains. The area selected for electron irradiation is marked with an open rectangle within the twin-free region. The magnetic behavior of the crystal was investigated by magneto-optical (MO) imaging of the emerging Meissner-state field expulsion upon cooling through T_c in the presence of a small applied magnetic field. Seen from the MO image in Fig. 1(b) taken at 76 K, the crystal has excellent magnetic uniformity as judged by its homogeneous contrast. The uniformity is at μm scale, limited largely by the resolution of optical microscope. Such uniform field expulsion persists even at 86 K, which is very close to the onset T_c of 93 K determined based on a series of MO images as temperature changes. From dc magnetization measurements under an applied external field $H_{\text{ext}}\approx0.1$ Oe, the onset T_c is ~93 K with a sharp transition of width ~0.5 K. This largely suggests optimal oxygen doping with $\delta\approx0.08$. However, even at this low field, the zero-field cooled $M(T)$ curve carries a long tail dragging from 55 to 92.5 K in which $\chi=M(T)/H_{\text{ext}}$ varies by ~20% from $\chi\approx-1$ to ≈-0.8. Increase of the applied external field to 1 Oe widens the transition width slightly, but a similar $M(T)$ tail persists over the same temperature range. Despite the μm level magneto-optic uniformity, these long $M(T)$ tails point

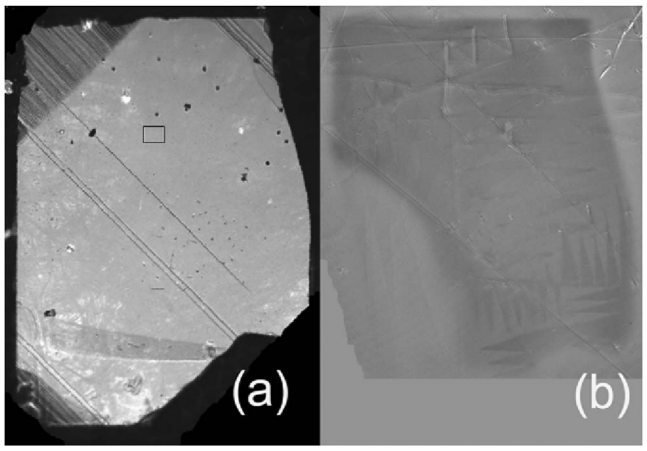

FIG. 1. (a) Picture of the YBCO cystal taken with a polarizing microscope revealing a large central part essentially free of twins and surrounded by heavily twinned corner regions with twin boundaries along the [110] direction. The straight sample edges are along the *a* or *b* axis. The rectangle marks where the electron bombardment and later Raman spectroscopy measurements were carried out. (b) MO image of the sample, after the lower left corner was accidentally chipped off. The image shows a uniform flux expulsion in the superconductor at 76 K during cooling in the presence of an external field of 100 Oe. Note that the zigzag pattern is not from the sample, but stems from magnetic domains in the ferrite garnet film used as Faraday-active indicator in the MO imaging.

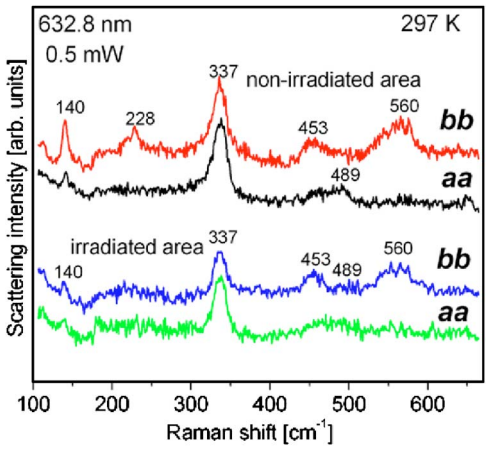

FIG. 2. (Color online) Polarized Raman spectra from the twin-free YBCO crystal in the irradiated and nonirradiated areas. The peaks at 140 cm^{-1}, 337 cm^{-1}, and 489 cm^{-1} correspond to the T (or T'), ortho-I, and ortho-II phases, respectively. The peak at 228-cm^{-1} represents the vibration of Cu atoms at chain ends, the number of which measured by the peak intensity. The diminution of this peak hence suggests the lengthening of $[\text{-Cu(1)-O(1)-}]_n$ chains with overall oxygen content kept unchanged.

to the submicron inhomogeneities of oxygen stoichiometry or the uneven distribution of oxygen point defects, with the variation of δ ranging from ~ 0.08 to ~ 0.4 over the entire sample. The volume fraction of each composition decreases continuously with increasing degree of oxygen deficiency. One has $\delta \approx 0.08$ for the most part, but $\delta \approx 0.08-0.4$ for the rest.

For electron irradiation, a field-emission scanning electron microscope was used to provide the 20-keV electron beam. The beam, perpendicularly incident on the crystal plate, was focused into a spot size of 70 nm in diameter and scanned over an area of 10×10 μm^2. The beam current density was about 3×10^{19} electrons/s cm^2, summing up to an overall dosage of approximately $3.5 \times 10^{18}/cm^2$ after 30 s of exposure per electron beam spot at 1 μm intervals over the entire 10×10 μm^2 scanned region, giving a total of 100 spots over a 50-min period. The 1-μm intervals should give reasonably uniform overall coverage as lateral scattering of the electrons would lead to a 3-D straggling of similar length scale.

Micro-Raman spectra were measured using the 632.8-nm excitation of a He-Ne laser with *aa* and *bb* scattering configurations, where the incident and scattered polarizations are both parallel to either the *a* or the *b* axis, respectively. We used 0.5-mW laser power together with an integration time of 45 min. The low laser power was adopted to avoid possible complications from competing photoinduced ordering effects during the long integration time. The Raman data represent the top 60-nm skin depth layer of the sample, where the effect of the electron irradiation is expected to be uniform.

Figure 2 shows the *aa* and *bb* polarized spectra measured at room temperature on the area that was electron irradiated, together with the results obtained from an adjacent unirradiated area. The distinctive spectral profiles of the *aa* and *bb* spectra allow for an unambiguous identification of the *a* and *b* directions.[12,13] At microscopic level, the structure of oxygen-deficient YBCO is characterized by the coexistence of submicrodomains (or "submicrophases") of different oxygen arrangements (ortho-I, ortho-II, T, T').[14] The Raman spectrum therefore is a superposition of the spectra of these coexisting phases, with the relative weight of each phase being determined by its abundance and Raman cross section.[14–18] The Raman peak at 140 cm^{-1}, representing the mode of Cu(2) vibrations along the *c* axis, is dominated by contributions from the tetragonal $T(\delta=1)$ and T' phases $(0<\delta<1)$, and also from partial oxygen disorder. Meanwhile, the position of the O(2),O(3) out-of-phase peak (337 cm^{-1}) is indicative of the contributions from ortho-I submicrodomains, whereas the O(2),O(3) in-phase mode at 453 cm^{-1} is suggestive of the ortho-II or T phase.[16] The presence of ortho-II phase ($\delta=0.33$) is also supported by the ortho-II apex oxygen (O4) peak at 489 cm^{-1}.[15,16]

The narrow peak at 228 cm^{-1} and the broad band centered at ~ 560 cm^{-1} are observed only in the *bb* spectra and cannot be assigned to any of the Raman-allowed modes of the ortho-I ($\delta=0.5$), ortho-II, or T submicrophases. Wake *et al.*[9] studied the 228-cm^{-1} peak for untwinned YBCO crystals in which it was established that the peak appears strictly when the light wave is *bb*-polarized and has a sharp resonance for laser energies near 2.2 eV (ours being 1.96 eV). On the basis of their laser annealing experiments, carried out using a 2.18 eV excitation, Iliev *et al.*[16] concluded that this peak was related to the vibrations of chain-end atoms and its intensity reflected the number of chain fragments rather than the overall oxygen content. Thus, the diminution of the 228-cm^{-1} peak after electron bombardment is a manifestation of a dra-

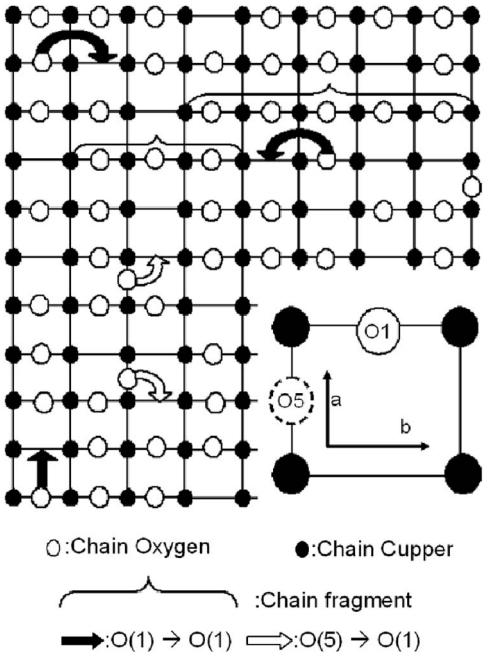

FIG. 3. Schematics of an oxygen-deficient twin-free YBCO basal plane (partially T' phase), showing (i) the definition of a and b axes of a perfect lattice (bottom right), and (ii) various locations of oxygen atoms, vacancies, interstitials, and their motions that effect the ordering. Arrows correspond to the movements of oxygen.

matically reduced number of chain ends. Given constant oxygen content, this then translates into the elongation of chain fragments. The relative weight of the chain ends would hence have to decrease, as indeed is the case and is corroborated by the decrease in intensity of the 140-cm^{-1} peak assigned to the oxygen-disordered T' phase. To be more specific, the healing process occurs through the irradiation-instigated collective transfer of oxygen atoms either from occupied O(5) interstitial sites to O(1) vacancy sites or by rearrangements of the $[\text{-Cu(1)-O(1)-}]_n$ chain segments such that their average length n ultimately increases at the expense of the total number. Figure 3 illustrates these possible ordering processes.

One key question is why the 20-keV electron irradiation leads to the relocation of oxygen atoms and enhanced ordering. Thermally activated kinetics alone cannot give a full account because all processes take place at room temperature. To seek a more comprehensive answer, consider first the interpretation of persistent normal-state conductivity and enhanced T_c in YBCO superconductors as originating from photoexcitation-induced oxygen ordering.[1,23] Then, from the relativistic corpuscular momentum transfer of a two-particle system of electron and oxygen atom in collision, the maximal energy transferred to the host atom will be[19] $E_{\text{atom max}}=2M(E+2m_ec^2)E/[(m+M)^2c^2+2ME]$. Here E is the incident electron energy, M is the rest mass of the host atom, m_e is that of the electron, and c is the speed of light. The maximum energy would be transferred with a backscattering angle $\phi=180°$, which amounts to 2.79 eV for oxygen atoms, but less for other heavier atoms such as Cu, Y, and Ba from Rutherford scattering of the incident 20-keV electron. The reported enthalpy of bond formation for CuO is 270 kJ mol^{-1},[20] which is close to the 2.79 eV per CuO bond. In the literature, Cui *et al.*[21] assessed the energy to dislodge an oxygen atom from its lattice location to be approximately 1.4 eV. This being the case, then atomic oxygen migrations should occur if the scattering cross section is not taken into consideration. Nonetheless, considering all possible forms of inelastic scattering, starting from those of valence electrons to those of inner-shell electrons, the cross sections of scattering go as $\sigma_{\text{valence}}>\sigma_{\text{inner shell}}\gg\sigma_{\text{Rutherford}}$ $(\phi=180°)$.[22] We therefore assert that most of the energy transferred would go into ionizing the constituent atoms, rather than breaking the chemical bonds.

The bonding or valence electrons thus play a major role in the ensuing atomic rearrangements in the lattice. Inelastic scattering through core-level or valence electron excitations, for instance, may cause a temporal charge imbalance in the YBCO lattice to bring on the oxygen atomic rearrangements. In essence, a shift of electrochemical potential has occurred in the sample upon the electron beam exposure, an effect similar in spirit to the photoexcitation-induced charge ordering.[3] It is argued[1,23] that electron-hole pairs are created by photoexcitation in the CuO_2 planes, and the electrons of these pairs are then localized at oxygen vacancies, viz., empty O(1) sites in an ideal lattice, on the nearby partially oxidized Cu(1)O(1) chains. This process would tend to locally enhance the orthorhombic distortion that eventually triggers oxygen atoms to hop collectively from O(5) sites to neighboring O(1) sites, or from one O(1) site to another, as mentioned earlier, thus consummating the oxygen ordering effects. The same arguments should hold when the photons are substituted with electrons. Note that although the scattering cross section from an incident electron's collision with a free electron, σ_{elastic}, is larger than σ_{valence}, the free electron's effect on the later oxygen redistribution may be negligibly small because of the smaller role it plays in chemical bonding.[24] In addition, the heating effect by electron beams from phonon excitation, estimated to be $\sim$27 K, is also considered insignificant[25] in the present work.

In disordered states, oxygen vacancy concentration is directly related to the reduction in T_c compared with a fully oxygenated sample, at least on the underdoped side of the phase diagram. This is understandable as more vacancies means a larger number of broken chains. Indeed, Tolpygo *et al.*[11] found that electron irradiation led to chain-oxygen disordering for both optimally doped and underdoped YBCO samples, in which oxygen defects were responsible for the T_c reduction and electrical resistivity increases. However, the work was carried out on thin film samples with a 3–50 nA beam current and their dosages ranging from 10^{19} to 10^{21} electrons/cm^2, i.e., 15–250 times higher in beam current and 10^3–10^5 higher in dosage as compared to our irradiation conditions. Unfortunately, no observation was made in the dose limit that we used in the present work. Nevertheless, in Ref. 11(b) (Fig. 6), there in fact was sign of T_c enhancement as a consequence of irradiation even at relatively high dosages in their low-energy limit of 20–40 keV. In any event, the knock-out effect may not be negligible at their high dose extremes for energies greater than 40 keV, beyond which changes in T_c and normal-state resistivity

could have counteracted the concurrent oxygen ordering. Meanwhile, it is worth noting that our Raman results were reproducible over a 15-day room-temperature aging, though it is not yet clear as to why our sample demonstrated this extra resilience in comparison with earlier reports,[1–4,26] considering the commonly accepted high mobility of chain oxygen atoms.

In conclusion, we have studied the $[\text{-Cu(1)-O(1)-}]_n$ chain-oxygen ordering effect by irradiation of a twin-free $YBa_2Cu_3O_{7-\delta}$ single crystal with $\delta \sim 0.08-0.4$ using 20 -keV electron beams. Oxygen-deficient but twin-free YBCO $(0<\delta<1)$ samples may be a mixture of submicrodomains of structural phases of different degrees of oxygen deficiency averaged out to the observed δ, each with its different arrangements of the O(1) and O(5) sites and chain fragments in accordance with the local stoichiometry. Based on this notion, then nominally twin-free YBCO crystals of a specific oxygen content may actually contains nano- or submicrometer-scale short-range order or disorder. Electron irradiation causes an ordering process to commence. In our case, the resulting ordered phase appears to sustain prolonged room-temperature aging without showing any relapse of disordering. This opens up the possibilities of tailoring the oxygen order-disorder transition, i.e., manipulating the segmentation of the chain oxygen in a controllable fashion to acquire the desired T_c, especially by use of commercially available scanning electron microscopes. Use of electron excitations to induce oxygen ordering is an especially enticing approach as the state-of-the-art electron beams can be narrowed to a spot size of $\sim 1-10$ nm and nanopatterning is thus possible in an electron nanoscopic setting.

The authors are thankful to J. K. Meen and R. P. Sharma for useful discussions. Assistance on superconducting quantum interference device based dc magnetization measurement by Andrei Baikalov and Y. Y. Xue is also acknowledged. This work was supported in part by the State of Texas through the Texas Center for Superconductivity at the University of Houston and in part by National Science Foundation under Grant No. DMR0404542. Supports by the Welch Foundation and Norwegian Research Council are also acknowledged.

*Email: hseo@uh.edu
†Corresponding author. Email: qchen@uh.edu
‡Present address: Department of Physics, University of Regina, Regina, SK S4S 0A2, Canada.

[1] E. Osquiguil *et al.*, Phys. Rev. B **49**, 3675 (1994).
[2] A. Fainstein, P. Etchegoin, and J. Guimpel, Phys. Rev. B **58**, 9433 (1998).
[3] S. Bahrs *et al.*, Phys. Rev. B **70**, 014512 (2004), references therein.
[4] A. A. Aligia and J. Garces, Phys. Rev. B **49**, 524 (1994).
[5] D. de Fontaine, L. T. Wille, and S. C. Moss, Phys. Rev. B **36**, R5709 (1987); E. Salomons and D. de Fontaine, *ibid.* **41**, 11159 (1990).
[6] V. Plakhty *et al.*, Solid State Commun. **84**, 639 (1992); A. Stratilatov, V. Plakhty, Yu. Chernenkov, and V. Fedorov, Phys. Lett. A **180**, 137 (1993); P. Schleger *et al.*, Physica C **241**, 103 (1995).
[7] R. Beyers *et al.*, Nature (London) **340**, 619 (1989).
[8] P. Manca *et al.*, Phys. Rev. B **63**, 134512 (2001), and references therein.
[9] D. R. Wake, F. Slakey, M. V. Klein, J. P. Rice, and D. M. Ginsberg, Phys. Rev. Lett. **67**, 3728 (1991).
[10] J. Giapintzakis, D. M. Ginsberg, M. A. Kirk, and S. Ockers, Phys. Rev. B **50**, 15967 (1994); J. A. Fendrich *et al.*, Phys. Rev. Lett. **74**, 1210 (1995); Terukazu Nishizaki, Tomoyuki Naito, Satoru Okayasu, Akihiro Iwase, and Norio Kobayashi, Phys. Rev. B **61**, 3649 (2000).
[11] (a) S. N. Basu, T. E. Mitchell, and M. Nastasi, J. Appl. Phys. **69**, 3167 (1991); (b) S. K. Tolpygo, J. Y. Lin, M. Gurvitch, S. Y. Hou, and J. M. Phillips, Phys. Rev. B **53**, 12462 (1996); (c) S. K. Tolpygo *et al.*, Appl. Phys. Lett. **63**, 1696 (1993).
[12] F. Slakey, S. L. Cooper, M. V. Klein, J. P. Rice, and D. M. Ginsberg, Phys. Rev. B **39**, 2781 (1989).
[13] C. Thomsen, M. Cardona, B. Gegenheimer, R. Liu, and A. Simon, Phys. Rev. B **37**, 9860 (1988).
[14] M. N. Iliev, in *Spectroscopy of Superconducting Materials*, edited by Eric Faulques (American Chemical Society, Washington, DC, 1999).
[15] M. Iliev, C. Thomsen, V. Hadjiev, and M. Cardona, Phys. Rev. B **47**, 12341 (1993).
[16] M. N. Iliev, H.-U. Habermeier, M. Cardona, V. G. Hadjiev, and R. Gajic, Physica C **279**, 63 (1997).
[17] M. N. Iliev, P. X. Zhang, H.-U. Habermeier, and M. Cardona, J. Alloys Compd. **251**, 99 (1997).
[18] V. Venkataraman *et al.*, Physica C **402**, 1 (2004).
[19] H. Goldstein, C. P. Pole, and J. L. Safko, *Classical Mechanics*, 3rd ed. (Addison-Wesley, San Francisco, 2002).
[20] *CRC Handbook of Chemistry and Physics*, edited by D. R. Lide (CRC Press, Boca Raton, FL, 2000).
[21] F. Z. Cui, J. Xie, and H. D. Li, Phys. Rev. B **46**, 11182 (1992).
[22] L. Reimer, *Scanning Electron Microscopy*, Physics of Image Formation and Microanalysis vol. 45 (Springer, New York, 1998).
[23] G. Yu, C. H. Lee, A. J. Heeger, N. Herron, and E. M. McCarron, Phys. Rev. Lett. **67**, 2581 (1991).
[24] Joseph I. Goldstein *et al.*, *Scanning Electron Microscopy and X-Ray Microanalysis* (Plenum Press, New York, 1992).
[25] P. J. Potts, *Handbook of Rock Analysis* (Blackie & Son, London, 1987).
[26] G. Nieva *et al.*, Appl. Phys. Lett. **60**, 2159 (1992).